Title

Photoacid-Modified Nafion Membrane Morphology Determined by Resonant X–ray Scattering and Spectroscopy

Journal

ACS Macro Letters, 8(10)

ISSN

2161-1653

Authors

Su, Gregory M

White, William

Renna, Lawrence A

et al.

Publication Date

2019-10-15

DOI

10.1021/acsmacrolett.9b00622

Peer reviewed

Photoacid-Modified Nafion Membrane Morphology Determined by Resonant X-ray Scattering and Spectroscopy

Gregory M. Su,[*,†] William White,[‡] Lawrence A. Renna,[‡] Jun Feng,[†] Shane Ardo,[‡,¶,§] and Cheng Wang[*,†]

†*Advanced Light Source, Lawrence Berkeley National Laboratory, Berkeley, CA 94720, USA.*

‡*Department of Chemistry, University of California Irvine, Irvine, CA 92697, USA.*

¶*Department of Chemical Engineering & Biomolecular Engineering, University of California Irvine, Irvine, CA 92697, USA.*

§*Department of Materials Science & Engineering, University of California Irvine, Irvine, CA 92697, USA.*

E-mail: gsu@lbl.gov; cwang2@lbl.gov

Abstract

Covalent attachment of photoacid dye molecules to perfluorinated sulfonic acid membranes is a promising route to enable active light-driven ion pumps, but the complex relationship between chemical modification and morphology is not well understood in this class of functional materials. In this study, we demonstrate the effect of bound photoacid dyes on phase-segregated membrane morphology. Resonant X-ray scattering near the sulfur K-edge reveals that the introduction of photoacid dyes at the end of ionomer side-chains enhances phase segregation among ionomer domains,

and the ionomer domain spacing increases with increasing amount of bound dye. Furthermore, relative crystallinity is marginally enhanced within semicrystalline domains composed of the perfluorinated backbone. X-ray absorption spectroscopy coupled with first-principles density functional theory calculations suggest that above a critical concentration, the multiple hydrophilic groups of the attached photoacid dye may help increase residual water content and promote hydration of adjacent sulfonic acid side-chains under dry, or ambient, conditions.

Synthetic ion-conducting membranes are essential to electochemical applications including fuel cells, electrodialysis technologies, electrolyzers, and redox flow batteries.[1–8] In addition, the transport of ions across membranes is critical to many life processes. In some cells, light-driven ion pumps actively transport protons against a concentration gradient to drive synthesis of adenosine triphosphate (ATP).[9,10] Designing nature-inspired artificial light-harvesting systems could enable advances in energy conversion devices and reduce power consumption in electrolytic acid and base generation and electrodialysis. There has been significant work to develop artificial light-driven ion pumps.[9,11–17] Polymer-based membranes offer unique advantages because ion-conducting polymers exhibit excellent chemical stability, good mechanical properties, near single-charge-type conductivity, and can be transparent to visible light. We recently demonstrated photovoltaic action from perfluorosulfonic acid (PFSA) ionomer (Nafion) membranes with photoacid dye molecules covalently bound to the side-chain,[15] and lamination to an anion-exchange membrane produced bipolar membranes that convert sunlight to ionic power, showing promise for solar-driven desalination.[16]

The phase segregated morphology of perfluorinated ionomers dictates its ion transport, but morphology evolution due to covalent attachment of dyes remains unknown. The nanodomain structure is driven by incompatibility between the hydrophobic perfluorinated backbone and the hydrophilic side-chains.[1,18] Morphology is difficult to understand even for well-studied PFSAs like Nafion,[1,2] and advanced characterization tools are required to probe these chemically heterogeneous materials. Small-angle X-ray scattering (SAXS) can reveal

characteristic length scales on the order of nanometers associated with the distances between hydrophilic ionomer or perfluorinated semicrystalline domains. However, PFSA membranes are quite disordered and have limited elemental contrast resulting in broad scattering peaks. Complementary to SAXS, wide angle X-ray scattering (WAXS) probes Angstrom-scale periodicities relevant to the interchain packing distance in polymer crystallites.[1,19,20] Photoacid-modified PFSAs have additional chemical moieties making these materials more complex than the parent PFSA and more challenging to understand internal morphology.

X-rays at energies near the absorption edge of a relevant element in a polymer, e.g. carbon, can achieve elemental sensitivity and greater scattering contrast compared to higher energy hard X-rays and help elucidate morphological details in disordered membranes with multiple chemical motifs. Energy-tunable resonant X-ray scattering (RXS) has become indispensable to understanding polymer morphology,[21–23] but the vast majority of these studies have focused on polymer thin films using resonant soft X-ray scattering at energies near the carbon K-edge.[24–28] The limited penetration of soft X-rays restricts transmission-based experiments to thin films, for example, around 500 nm or less near the carbon K-edge ($\sim$285 eV). These low energy X-rays, which have a wavelength around 4 nm at 300 eV, cannot easily probe length-scale periodicities smaller than this size. Furthermore, the prevalence of carbon in polymers can make it difficult to delineate information specific to certain functional groups when working near the carbon K-edge, requiring tuning to other elemental edges, especially when combining RXS with near edge X-ray absorption fine structure (NEXAFS) spectroscopy to gain chemical and local bonding information.[21,29–32] For PFSA-based polymers, sulfur is important because it is only present in the ionic groups that contain dissociable protons. However, very limited studies have implemented RXS at energies near the sulfur K-edge to investigate polymeric materials in general.[33–35]

In this study, we show that attachment of photoacid dyes to Nafion alters ionomer domain spacing and short-range order. RXS in the tender X-ray regime, which includes the sulfur K-edge (around 2.5 keV or 0.5 nm), has enhanced contrast due to the presence of

sulfur-containing functional groups on both the Nafion side-chain (sulfonate) and the attached photoacid dye (sulfonamide), and this enables probing of internal morphology. This energy, or wavelength, range permits transmission RXS experiments on membranes that are 10's of micrometers thick and can probe domain spacings with nanometer resolution, relevant to ionomer phase-segregated morphologies. In addition, hard X-ray WAXS reveals that attachment of photoacid dyes moderately increases the relative crystallinity within semicrystalline polytetrafluoroethylene (PTFE) domains. Furthermore, sulfur K-edge NEXAFS spectroscopy and complementary ab initio calculations support the presence of covalently bound dyes and suggest that the membrane with the highest amount of attached dye may have increased residual water in the dry state that also facilitates hydration of nearby sulfonic acid side-chains. Resonant scattering and spectroscopy have the potential to provide insights on the spatial distribution of distinct chemical moieties not only for the dye-modified membranes studied here, but also other photoacid/photobase-doped materials,[36] soft materials, inorganic materials, and other chemically-heterogeneous systems.

The covalently modified PFSA (cPFSA) membranes studied herein were synthesized similarly to a previous report,[15] but vary in the type or equivalents of compounds used (Figure 1): equivalents of photoacid dye (D) molecule (0.1 or 2.0 equivalents), type of Lewis base (B) used to scavenge formed acid (100 equivalents of triethylamine (TEA) or diisopropylethylamine (DIPEA)), and equivalents of Brønsted-Lowry base (OH) (0 or 5 equivalents of NaOH). Equivalents represent the molar ratio of added material to the number of sulfonyl fluoride groups in the Nafion sulfonyl fluoride (-SO_2F) precursor membrane. Table 1 lists cPFSA membrane short and long names, and formulation details. The cPFSA membranes will be referred to by their short names. The overall trend in the amount of bound dye (DhBnb > DlBnbOH > DlBbOH) is evident by the color of the membranes, which are red, orange, and yellow for DhBnb, DlBnbOH, and DlBbOH, respectively (see Figure S1). Further synthetic details are provided in the Supporting Information.

Covalent attachment of photoacid dyes promotes a phase-segregated morphology with a

Table 1: Naming details and formulations of the cPFSA membranes used in this study

Short name	Long name	Details
DhBnb	cPFSA+Dye$_{high}$+Base$_{nonbulky}$	2.0 equiv. photoacid dye, 100 equiv. nonbulky TEA, 0 equiv. NaOH
DlBnbOH	cPFSA+Dye$_{low}$+Base$_{nonbulky}$+NaOH	0.1 equiv. photoacid dye, 100 equiv. nonbulky TEA, 5 equiv. NaOH
DlBbOH	cPFSA+Dye$_{low}$+Base$_{bulky}$+NaOH	0.1 equiv. photoacid dye, 100 equiv. bulky DIPEA, 5 equiv. NaOH

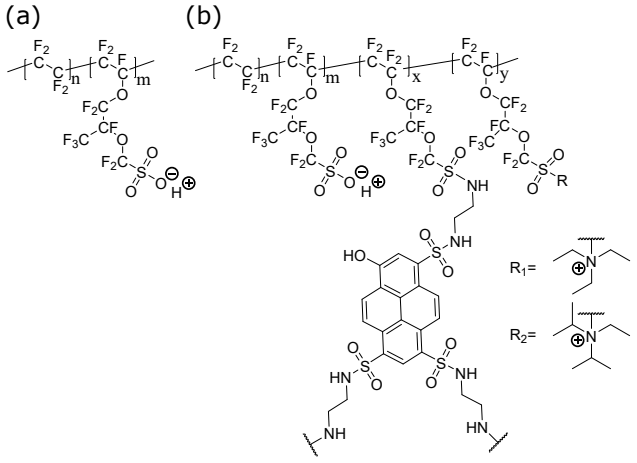

Figure 1: Chemical structures of the perfluorinated ionomers in this work. Nafion is shown in (a). The proposed structure of the cPFSA ionomers is shown in (b). DhBnb contains the most bound dyes, suggesting its value of x is largest. DhBnb and DlBnbOH were synthesized with the Lewis base triethylamine as an acid scavenger, forming R_1 groups. DlBbOH was synthesized using the bulkier diisopropylethylamine as an acid scavenger, forming R_2 groups.

domain spacing that increases with increasing amount of bound dye. PFSAs can be difficult to study with hard X-ray SAXS due to low material contrast relative to the topological scattering background (Figure S2). Furthermore, scattering intensity is weak because of the disordered nature of these materials and the membrane thickness (50 μm), which is thin for hard X-ray transmission experiments. On the other hand, a 50 μm membrane is too thick for transmission-based resonant scattering with lower energy soft X-rays, which have limited penetration. RXS at the sulfur K-edge addresses these issues. Significant absorption (around 2480 eV) due to sulfur causes variations in the complex index of refraction as a function of X-ray energy, considerably increasing scattering contrast, as shown in Figure 2a-b. RXS of the

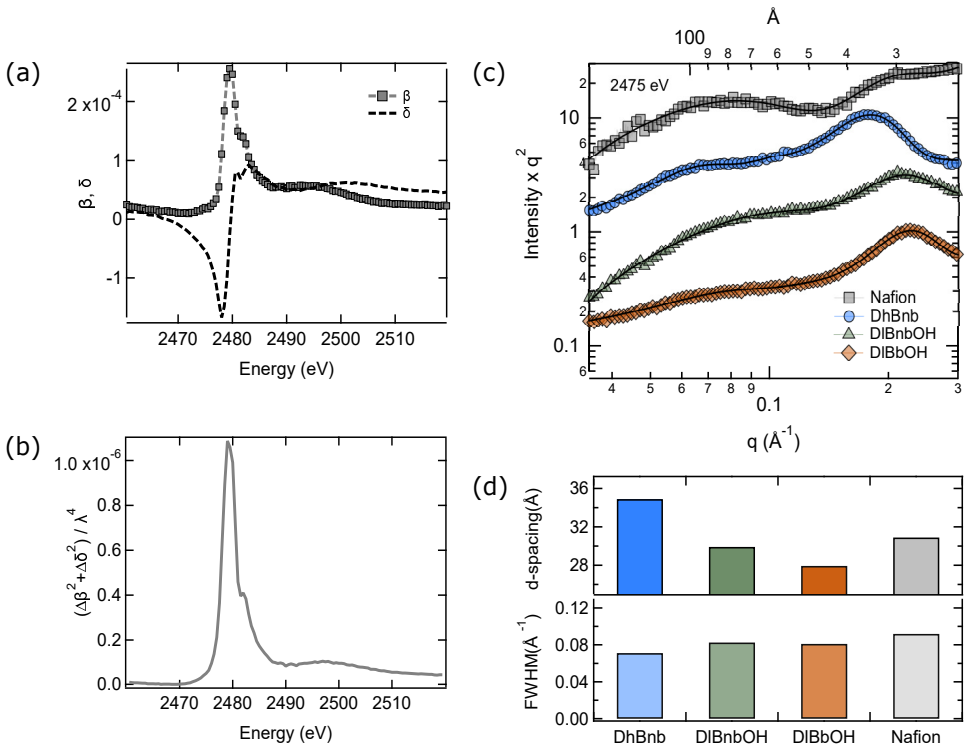

Figure 2: (a) Energy-dependent absorption, β, and dispersion, δ, components of the complex index of refraction. (b) Calculated scattering contrast as a function of energy. Data in (a) and (b) are representative for Nafion. Radially averaged, Lorentz-corrected transmission resonant X-ray scattering profiles at 2475 eV are shown in (c), and the curves are shifted vertically for ease of visibility. The solid black traces represent fits. The d-spacing and FWHM values determined from the fits are shown in (d) for the ionomer peak near 0.2 Å^{-1}.

cPFSA membranes is shown in Figure 2c at 2475 eV, an energy where contrast is enhanced, but below the main absorption peak to avoid excessive damage. The scattering profiles exhibit two distinct features typically seen for PFSAs: a peak at around $q = 0.06$ Å^{-1} representative of the average distance among semicrystalline domains, with a correlation length, or d-spacing ($2\pi/q$), of around 100 Å, and another peak at higher q near 0.2 Å^{-1} corresponding to approximately 30 Å, indicative of the spacing among hydrophlic ionomer domains, often referred to as the ionomer peak.[1] Bound photoacid dyes enhance phase segregation, as seen by the more pronounced ionomer peak in cPFSA membranes compared to Nafion. Among the cPFSA membranes, the ionomer domain d-spacing increases with increasing amount of bound dye with $d_{DhBnb} = 34.9$ Å $> d_{DlBnbOH} = 29.2$ Å $> d_{DlBbOH} = 27.9$ Å, as shown in Figure 2d. This implies that the ionomer phase segregation length-scale can be tuned

based on the amount of attached dye. Interestingly, the ionmoer d-spacing of Nafion is 30.9 Å, which is in the middle of this range. However, the ionomer scattering peak of Nafion is much less pronounced, making a d-spacing value more difficult to quantify. This trend in domain spacings of cPFSAs compared to Nafion underscores the complex interplay between changes in molecular structure and resulting phase-segregated morphology, illustrating the need for further detailed characterization going forward. The presence of dye also affects the short-range order among separate hydrophilic ionomer domains. DhBnb exhibits an ionomer scattering peak with the smallest full width at half maximum (FWHM) value, suggesting improved short-range order and/or a smaller distribution of domain sizes compared to DlBnbOH, DlBbOH, and Nafion. This is likely linked to the greater amount of bound dye in DhBnb. Overall, resonant scattering reveals how molecular moieties attached to the end of the side-chains of a PFSA ionomer alter the nanoscale phase-segregated morphology and the correlation lengths among ionomer domains, and this can be tuned based on the concentration of bound dye molecules.

The presence of photoacid dyes and molecules bound to form sulfonamide-linked cationic groups (Figure 1b) may also affect correlations among semicrystalline domains. Among the cPFSA membranes investigated, the broad semicrystalline correlation feature centered near 0.06 $Å^{-1}$ is moderately more pronounced for DhBnb, which has the greaest amount of bound dye, suggesting a greater degree of short-range order among its semicrystalline PTFE domains, as shown in Figure 2c. DlBbOH, on the other hand, has the least amount of bound dye and a larger sulfonamide-linked cationic group from the bulkier DIPEA Brønsted-Lowry base used in its formulation, which may inhibit ordering even among semicrystalline domains. Figure 2c shows that DlBbOH has a semicrystalline peak that is noticeably less pronounced, indicative of greater disorder among its semicrystalline domains. Multiple effects including the amount of added dye and the size of the sulfonamide-linked cationic group likely contribute to the overall semicrystalline inter-domain structure. In general, dye molecules have the potential to induce ordering among both ionomer and semicrystalline phases in

dye-modified Nafion membranes. The elemental and chemical sensitivity provided by resonant scattering can probe morphological details beyond what is possible with hard X-ray (off-resonance) scattering. Going forward, new insights on nanoscale structure, for example, the degree of spatial homogeneity in the distribution of sulfur-containing functional groups within hydrophilic domains and how this evolves with increasing hydration, will require well-defined materials and advanced *in situ* studies.

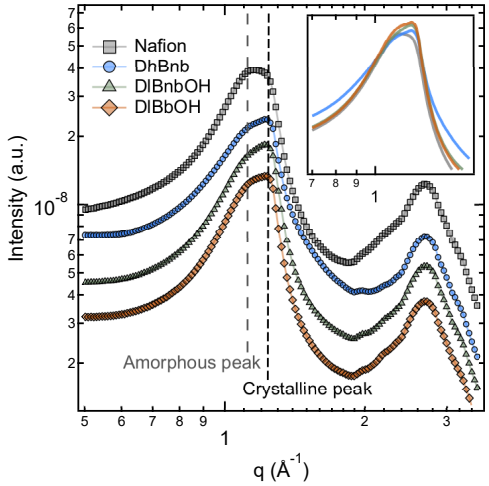

Figure 3: Hard X-ray transmission wide-angle X-ray scattering profiles of Nafion and cPFSA membranes. Scattering curves are shifted vertically for ease of visibility. Inset shows a zoom-in of the crystalline peak with no offset.

Individual semicrystalline PTFE domains consist of regions of both amorphous polymer backbone chains and ordered crystallites, and WAXS data suggest that dye molecules at the end of PFSA side-chains promotes backbone (PTFE-based) crystallization. WAXS provides Angstrom-scale molecular packing information, relevant to the distance between polymer chains within PTFE crystallites.[1,19,37] This compliments RXS experiments, which cannot easily probe these small length-scales. WAXS profiles for Nafion and the cPFSA membranes are shown in Figure 3, and two main features are observed, one around 1.0-1.3 $Å^{-1}$ and another near 2.4-3.0 $Å^{-1}$, similar to previous reports on Nafion.[38] The feature centered near 1.2 $Å^{-1}$ is typically seen for semicrystalline PTFE and consists of two peaks close together. The broader amorphous peak at 1.15 $Å^{-1}$ arises due to short-range correlations among disordered polymer chains, and this is superimposed with a crystalline peak at 1.25 $Å^{-1}$

corresponding to the intermolecular chain spacing within crystallites that is typically strong for pristine PTFE,[37] and weaker but still noticeable in PFSAs.[19,38,39] cPFSA membranes have enhanced crystallinity within semicrystalline PTFE-based backbone-rich domains compared to the Nafion used in this work. This is evident by the greater relative intensity of the crystalline peak compared to the amorphous peak in the cPFSA membranes. By fitting the semicrystalline feature to two peaks, an amorphous peak centered near 1.15 $Å^{-1}$ and a crystalline peak at 1.25 $Å^{-1}$, the relative crystallinity, χ_c, was estimated by the ratio of the area of crystalline peak, A_c, to the total area of the amorphous peak, A_a, and the crystalline peak: $\chi_c = A_c/(A_a + A_c)$. This is shown in Figure S8. The cPFSA membranes have χ_c values of 0.20, 0.12, and 0.13 for DhBnb, DlBnbOH, and DlBbOH, respectively. Nafion has a noticeably lower χ_c value of 0.05. The presence of hydrophilic photoacid moieties increases the segregation of ionomer domains, as seen from the RXS in Figure 2c, and this may also allow perfluorinated backbone segments to pack and crystallize more easily within semicrystalline regions. However, a more detailed understanding of this effect would require additional work including *in situ* experiments. The second main feature present in the WAXS data at higher q (2.4-3.0 $Å^{-1}$) has been reported previously for Nafion and attributed to various intrachain correlations along the backbone that superimpose into a broad feature.[38] No significant change in this feature is evident among Nafion and the cPFSA membranes.

NEXAFS spectroscopy can probe differences in molecular structure among different perfluorinated ionomers,[35,40–42] and NEXAFS at the sulfur K-edge, which is sensitive to the local environment around the sulfonate and sulfonamide functional groups, supports that DhBnb has the greatest amount of bound dye and may have greater residual water. Experimental NEXAFS spectra for Nafion and the cPFSA membranes are shown in Figure 4a. The main absorption features are similar to previous reports of PFSA polymers.[41,42] For PFSAs, the main peak near 2480 eV has been assigned to a σ^*_{S-C} transition,[41,43] however, multiple electronic transitions may be superimposed within this broad peak that are difficult to discern experimentally. Figure 4a reveals that the NEXAFS spectrum of the dye precursor does

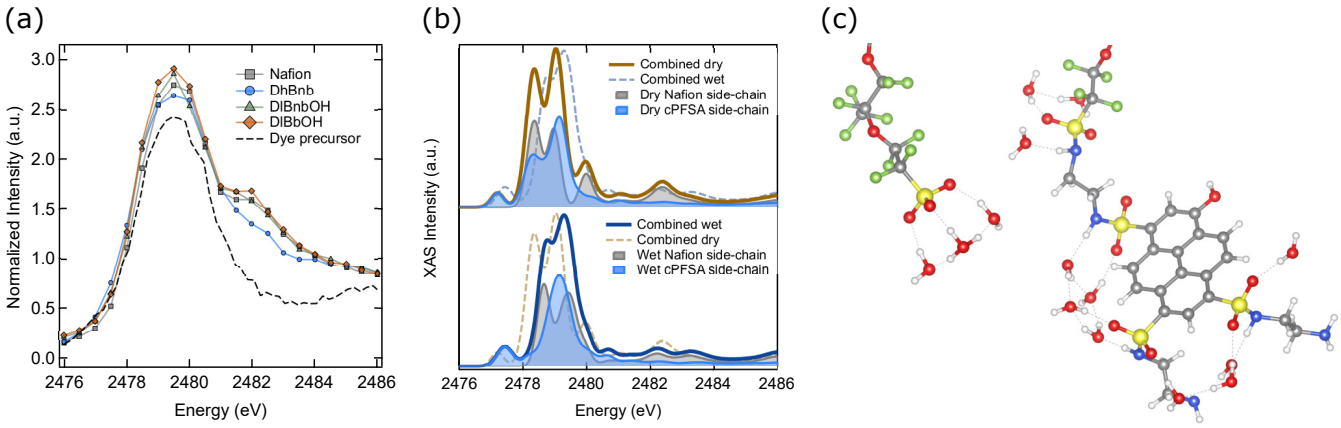

Figure 4: Sulfur K-edge NEXAFS spectra collected in fluorescence detection mode for Nafion, cPFSA membranes, and the dye precursor are shown in (a). Simulated NEXAFS spectra for dry (no added water) and minimally hydrated side-chains are shown in (b). Separate spectra are shown for PFSA (SO_3H-terminated) and photoacid-modified side-chains. Solid lines (combined) show the equally weighted sum of spectra of both side-chain types. Dry and hydrated combined spectra are replotted in opposing panels as dotted lines for comparison. Optimized minimum energy structures of the hydrated Nafion side-chain (group m in Figure 1) and photoacid-modified side-chain (group x in Figure 1) are shown in (c).

not exhibit a shoulder-like feature near 2482 eV. DhBnb exhibits a less pronounced shoulder feature near 2482 eV compared to DlBnbOH and DlBbOH, supporting that DhBnb contains the highest concentration of photoacid dyes. Furthermore, this distinction in the NEXAFS profile of DhBnb may also be related to a different degree of hydration, or residual water content. Although these membranes were annealed at 90 °C before being measured under ambient conditions, some water molecules remain strongly bound to the sulfonic acid and sulfonamide groups, and residual water is typically observed for PFSAs like Nafion.[1] Earlier studies show that when Nafion is hydrated, the energy separation between the shoulder feature and main absorption peak decreases, making the higher energy shoulder less pronounced.[41] The greater amount of attached dye in DhBnb may allow it to retain more water compared to Nafion and the other cPFSA membranes, even in dry, or ambient conditions. Future studies should correlate spectroscopy and scattering results to measurements of water uptake and molecular modeling to better understand the details of how bound photoacid dyes influence water sorption.

First-principles predictions of NEXAFS spectra help reveal how hydration leads to spectral changes. NEXAFS spectra were calculated using the eXcited electron and Core Hole (XCH) approach[44] based on density functional theory (DFT).[45,46] The XCH method has been shown to reproduce K-edge NEXAFS spectra of polymers,[29,30] and XCH-computed sulfur K-edge spectra of a perfluorinated fragment containing either a Nafion side-chain (-SO_3H terminated) or a photoacid-bound PFSA side-chain are shown in Figure 4b. Spectra were calculated for dehydrated side-chains or side-chains with water hydrogen bonded around the sulfonic acid and sulfonamide groups. The simulated combined spectra assume equal contributions from -SO_3H terminated and photoacid-bound side-chains, that is m = x based on Figure 1. The actual cPFSA membranes have differing m : x ratios and likely unequal amounts of sulfonic acid-terminated and photoacid-modified side-chains. Molecular geometries of the hydrated structures are shown in Figure 4c. The presence of water changes the simulated spectra. The main absorption feature, which contains two separate peaks, shifts to higher energy. The lowest energy transition near 2477.2 eV, which has relatively low intensity, and originates solely from photoacid-modified side-chains, also shifts to higher energy to around 2477.4 eV. Although this feature is unique to the dye, it is not obvious in the experimental data. This may be due to a low dye concentration and the possibility that calculations overestimate oscillator strengths. The states near 2477 eV unique to the photoacid dye likely represent coupling to the π^* system of the pyrenol-based core of the photoacid dye and a σ^*_{S-N} transition (Figure S5). Overall, it can be challenging experimentally to discern transitions that are either close together in energy or have low intensity, highlighting the importance of complementary insights from first-principles predictions.

Nafion (-SO_3H terminated side-chain) exhibits peaks near 2480 eV and 2482.4 eV in the computed spectra that become less pronounced when hydrated. This correlates with the experimental observation of DhBnb's reduced intensity of the shoulder feature in a similar energy range relative to the other membranes, suggesting that this difference in its NEXAFS spectrum may be due to not only the presence of a higher concentration of photoacid dye

in DhBnb, but also increased residual water. The XCH-computed spectra show that the features at 2480 eV and 2482.4 eV are mostly specific to Nafion-like side-chains, hence the reduced intensity of the broad shoulder feature exhibited by DhBnb suggests greater hydration in the Nafion segments of the copolymer. The higher concentration of attached dye in DhBnb could retain more water molecules under dry (ambient) conditions, and these water molecules can hydrate nearby Nafion-like (-SO_3H terminated) side-chains within the same ionomer domain. Previous modeling studies reveal that water molecules form hydrogen bonds that bridge acidic groups on adjacent side-chains in short side-chain PFSAs.[47] Greater residual water may play a role in driving the improved ordering among ionomer domains seen in DhBnb, and ordering typically increases with water content for PFSAs in general.[1] Residual water content is an important parameter to consider when designing ion-conducting polymers as it influences proton dissociation, domain network, and conductivity, especially under minimal hydration conditions.

This study provides new insights into the phase-segregated morphology evolution of photoacid-modified perfluorinated ionomer membranes. Covalent attachment of dye molecules enables these materials to act as light-driven ion pumps, but these changes affect critical aspects of morphology that dictate ion transport. Contrast-enhanced resonant X-ray scattering near sulfur K-edge energies reveals correlation lengths and ordering among ionomer and semicrystalline domains in Nafion membranes with varying amount of bound photoacid dye. The average spacing among ionomer domains increases with increasing amount of attached dye. The presence of dye molecules induces phase segregation and generally increases the local ordering among ionomer domains compared to Nafion. Furthermore, dye-containing ionomer membranes show a moderate increase in the relative crystallinity of PTFE-based crystallites within semicrystalline domains compared to Nafion, as shown by X-ray diffraction. Element-specific X-ray absorption spectroscopy coupled with first-principles calculations has the potential to provide insight into local water content and suggests that above a critical concentration of dye, additional residual water may be present and promote hy-

dration of both photoacid-terminated and sulfonic acid-terminated side-chains. Overall, this work highlights the interplay between chemical modification and nanoscale domain structure in perfluorinated ionomer membranes, and showcases the utility of elementally sensitive X-rays to probe chemistry and morphology. Chemically sensitive structural probes can play an important role in the design of new materials, and should be more closely coupled with ion conductivity measurements and other performance metrics going forward. This study establishes fundamental understanding to help guide rational development of polymers that can be used as light-driven ion pumps for solar-driven desalination and other applications.

Acknowledgement

WW, LAR, and SA acknowledge support from the Gordon & Betty Moore Foundation under a Moore Inventor Fellowship (GBMF grant No. 5641). GMS, JF, and CW acknowledge support from the Advanced Light Source. The use of the Advanced Light Source (ALS) including beamlines 5.3.1 (resonant X-ray scattering and spectroscopy at the sulfur K-edge) and 7.3.3 (hard X-ray SAXS/WAXS), a user project at The Molecular Foundry and use of its computer cluster Etna managed by the High Performance Computing Services Group, and the use of the National Energy Research Scientific Computing (NERSC) Center were performed at Lawrence Berkeley National Laboratory, which is supported by the Director, Office of Science, Office of Basic Energy Sciences, of the DOE under contract No. DE-AC02-05CH11231. Some preliminary resonant X-ray scattering measurements were perfomed under proposal number 2017G709 on beamline 15A2 at the Photon Factory, Japan.

Supporting Information Available

Materials, membrane formulation, experimental, and computational details, color change of cPFSA with dye loading, hard X-ray SAXS vs. RXS, low-q RXS data, energy-minimized geometries of dehydrated side-chains, representative data for RXS at different energies and

for separately synthesized cPFSA membranes, fits to WAXS data, attenuation length as a function of X-ray energy

References

(1) Kusoglu, A.; Weber, A. Z. New Insights into Perfluorinated Sulfonic-Acid Ionomers. *Chem. Rev.* **2017**, *117*, 987–1104.

(2) Mauritz, K. A.; Moore, R. B. State of Understanding of Nafion. *Chem. Rev.* **2004**, *104*, 4535–4586.

(3) Hamrock, S. J.; Yandrasits, M. A. Proton Exchange Membranes for Fuel Cell Applications. *J. Macromol. Sci. Polymer Rev.* **2006**, *46*, 219–244.

(4) Perry, M. L.; Weber, A. Z. Advanced Redox-Flow Batteries: A Perspective. *J. Electrochem. Soc.* **2016**, *163*, A5064–A506.

(5) Weber, A. Z.; Mench, M. M.; Meyers, J. P.; Ross, P. N.; Gostick, J. T.; Liu, Q. Redox flow batteries: a review. *J. Appl. Electrochem.* **2011**, *41*, 1137.

(6) Modestino, M. A.; Walczak, K. A.; Berger, A.; Evans, C. M.; Haussener, S.; Koval, C.; Newman, J. S.; Ager, J. W.; Segalman, R. A. Robust production of purified H_2 in a stable, self-regulating, and continuously operating solar fuel generator. *Energy Environ. Sci.* **2014**, *7*, 297–301.

(7) Rodriguez, C. A.; Modestino, M. A.; Psaltis, D.; Moser, C. Design and cost considerations for practical solar-hydrogen generators. *Energy Environ. Sci.* **2014**, *7*, 3828–3835.

(8) Xu, T. Ion exchange membranes: State of their development and perspective. *J. Membr. Sci.* **2005**, *263*, 1–29.

(9) Tributsch, H. Light driven proton pumps. *Ionics* **2000**, *6*, 161–171.

(10) Gadsby, D. C. Ion channels versus ion pumps: the principal difference, in principle. *Nat. Rev. Mol. Cell Biol.* **2009**, *10*, 344–352.

(11) Sun, K.; Mauzerall, D. A simple light-driven transmembrane proton pump. *Proc. Natl. Acad. Sci.* **1996**, *93*, 10758–10762.

(12) Steinberg-Yfrach, G.; Liddell, P. A.; Hung, S.-C.; Moore, A. L.; Gust, D.; Moore, T. A. Conversion of light energy to proton potential in liposomes by artificial photosynthetic reaction centres. *Nature* **1997**, *385*, 239–241.

(13) Bhosale, S.; Sisson, A. L.; Talukdar, P.; Fürstenberg, A.; Banerji, N.; Vauthey, E.; Bollot, G.; Mareda, J.; Röger, C.; Würthner, F.; Sakai, N.; Matile, S. Photoproduction of Proton Gradients with -Stacked Fluorophore Scaffolds in Lipid Bilayers. *Science* **2006**, *313*, 84–86.

(14) Xie, X.; Crespo, G. A.; Mistlberger, G.; E., B. Photocurrent generation based on a light-driven proton pump in an artificial liquid membrane. *Nat. Chem.* **2014**, *6*, 202–207.

(15) White, W.; Sanborn, C. D.; Reiter, R. S.; Fabian, D. M.; Ardo, S. Observation of Photovoltaic Action from Photoacid-Modified Nafion Due to Light-Driven Ion Transport. *J. Am. Chem. Soc.* **2017**, *139*, 11726–11733.

(16) White, W.; Sanborn, C. D.; Fabian, D. M.; Ardo, S. Conversion of Visible Light into Ionic Power Using Photoacid-Dye-Sensitized Bipolar Ion-Exchange Membranes. *Joule* **2018**, *2*, 94 – 109.

(17) Xiao, K.; Chen, L.; Heil, T.; Daniel Cruz Lemus, S.; Fan, F.; Wen, L.; Jiang, L.; Antonietti, M. Artificial light-driven ion pump for photoelectric energy conversion. *Nat. Commun.* **2019**, *10*, 74.

(18) Kusoglu, A.; Dursch, T. J.; Weber, A. Z. Nanostructure/Swelling Relationships of Bulk and Thin-Film PFSA Ionomers. *Adv. Funct. Mater.* **2016**, *26*, 4961–4975.

(19) Kusoglu, A.; Savagatrup, S.; Clark, K. T.; Weber, A. Z. Role of Mechanical Factors in Controlling the StructureFunction Relationship of PFSA Ionomers. *Macromolecules* **2012**, *45*, 7467–7476.

(20) Su, G. M.; Lim, E.; Jacobs, A. R.; Kramer, E. J.; Chabinyc, M. L. Polymer Side Chain Modification Alters Phase Separation in Ferroelectric-Semiconductor Polymer Blends for Organic Memory. *ACS Macro Lett.* **2014**, *3*, 1244–1248.

(21) Su, G. M.; Cordova, I. A.; Brady, M. A.; Prendergast, D.; Wang, C. Combining theory and experiment for X-ray absorption spectroscopy and resonant X-ray scattering characterization of polymers. *Polymer* **2016**, *99*, 782–796.

(22) Ade, H.; Hitchcock, A. P. NEXAFS microscopy and resonant scattering: Composition and orientation probed in real and reciprocal space. *Polymer* **2008**, *49*, 643–675.

(23) Liu, F.; Brady, M. A.; Wang, C. Resonant Soft X-ray Scattering for Polymer Materials. *Eur. Polym. J.* **2016**, *81*, 555–568.

(24) Wang, C.; Lee, D. H.; Hexemer, A.; Kim, M. I.; Zhao, W.; Hasegawa, H.; Ade, H.; Russell, T. P. Defining the Nanostructured Morphology of Triblock Copolymers Using Resonant Soft X-ray Scattering. *Nano Lett.* **2011**, *11*, 3906–3911.

(25) Culp, T. E.; Ye, D.; Paul, M.; Roy, A.; Behr, M. J.; Jons, S.; Rosenberg, S.; Wang, C.; Gomez, E. W.; Kumar, M.; Gomez, E. D. Probing the Internal Microstructure of Polyamide Thin-Film Composite Membranes Using Resonant Soft X-ray Scattering. *ACS Macro Lett.* **2018**, *7*, 927–932.

(26) Virgili, J. M.; Tao, Y.; Kortright, J. B.; Balsara, N. P.; Segalman, R. A. Analysis of

Order Formation in Block Copolymer Thin Films Using Resonant Soft X-ray Scattering. *Macromolecules* **2007**, *40*, 2092–2099.

(27) Litofsky, J. H.; Lee, Y.; Aplan, M. P.; Kuei, B.; Hexemer, A.; Wang, C.; Wang, Q.; Gomez, E. D. Polarized Soft X-ray Scattering Reveals Chain Orientation within Nanoscale Polymer Domains. *Macromolecules* **2019**, *52*, 2803–2813.

(28) Collins, B. A.; Cochran, J. E.; Yan, H.; Gann, E.; Hub, C.; Fink, R.; Wang, C.; Schuettfort, T.; McNeill, C. R.; Chabinyc, M. L.; Ade, H. Polarized X-ray scattering reveals non-crystalline orientational ordering in organic films. *Nat. Mater.* **2012**, *11*, 536–543.

(29) Patel, S. N.; Su, G. M.; Luo, C.; Wang, M.; Perez, L. A.; Fischer, D. A.; Prendergast, D.; Bazan, G. C.; Heeger, A. J.; Chabinyc, M. L.; Kramer, E. J. NEXAFS Spectroscopy Reveals the Molecular Orientation in Blade-Coated Pyridal[2,1,3]thiadiazole-Containing Conjugated Polymer Thin Films. *Macromolecules* **2015**, *48*, 6606–6616.

(30) Su, G. M.; Patel, S. N.; Pemmaraju, C. D.; Prendergast, D.; Chabinyc, M. L. First-Principles Predictions of Near-Edge X-ray Absorption Fine Structure Spectra of Semiconducting Polymers. *J. Phys. Chem. C* **2017**, *121*, 9142–9152.

(31) Kortright, J. B.; Sun, J.; Spencer, R. K.; Jiang, X.; Zuckermann, R. N. Oxygen K Edge Scattering from Bulk Comb Diblock Copolymer Reveals Extended, Ordered Backbones above Lamellar Order-Disorder Transition. *J. Phys. Chem. B* **2017**, *121*, 298–305.

(32) Ingham, B.; Smialowska, A.; Kirby, N. M.; Wang, C.; Carr, A. J. A structural comparison of casein micelles in cow, goat and sheep milk using X-ray scattering. *Soft Matter* **2018**, *14*, 3336–3343.

(33) Mårdalen, J.; Riekel, C.; Müller, H. Anomalous Xray scattering at the sulfur edge of poly(3-octylthiophene). *J. Appl. Cryst.* **1994**, *27*, 192–195.

(34) Coric, M.; Saxena, N.; Pflüger, M.; Müller-Buschbaum, P.; Krumrey, M.; Herzig, E. M. Resonant Grazing-Incidence Small-Angle X-ray Scattering at the Sulfur K-Edge for Material-Specific Investigation of Thin-Film Nanostructures. *J. Phys. Chem. Lett.* **2018**, *9*, 3081–3086.

(35) Su, G. M.; Cordova, I. A.; Yandrasits, M. A.; Lindell, M.; Feng, J.; Wang, C.; Kusoglu, A. Chemical and Morphological Origins of Improved Ion Conductivity in Perfluoro Ionene Chain Extended Ionomers. *J. Am. Chem. Soc.* **2019**, *141*, 13547–13561.

(36) Wang, L.; Wen, Q.; Jia, P.; Jia, M.; Lu, D.; Sun, X.; Jiang, L.; Guo, W. Light-Driven Active Proton Transport through Photoacid- and Photobase-Doped Janus Graphene Oxide Membranes. *Adv. Mater.* **2019**, 1903029.

(37) Lebedev, Y. A.; Korolev, Y. M.; Polikarpov, V. M.; Ignat'eva, L. N.; Antipov, E. M. X-ray powder diffraction study of polytetrafluoroethylene. *Crystallogr. Rep.* **2010**, *55*, 609–614.

(38) van der Heijden, P. C.; Rubatat, L.; Diat, O. Orientation of Drawn Nafion at Molecular and Mesoscopic Scales. *Macromolecules* **2004**, *37*, 5327–5336.

(39) Starkweather, H. W. Crystallinity in perfluorosulfonic acid ionomers and related polymers. *Macromolecules* **1982**, *15*, 320–323.

(40) Yan, Z. B.; Hayes, R.; Melo, L. G. A.; Goward, G. R.; Hitchcock, A. P. X-ray Absorption and Solid-State NMR Spectroscopy of Fluorinated Proton Conducting Polymers. *J. Phys. Chem. C* **2018**, *122*, 3233–3244.

(41) Isegawa, K.; Nagami, T.; Jomori, S.; Yoshida, M.; Kondoh, H. *In situ* S-K XANES study of polymer electrolyte fuel cells: changes in the chemical states of sulfonic groups depending on humidity. *Phys. Chem. Chem. Phys.* **2016**, *18*, 25183–25190.

(42) Vijayakumar, M.; Govind, N.; Li, B.; Wei, X.; Nie, Z.; Thevuthasan, S.; Sprenkle, V.; Wang, W. Aqua-Vanadyl Ion Interaction with Nafion Membranes. *Front. Energy Res.* **2015**, *3*, 10.

(43) Damian Risberg, E.; Eriksson, L.; Mink, J.; Pettersson, L. G. M.; Skripkin, M. Y.; Sandström, M. Sulfur X-ray Absorption and Vibrational Spectroscopic Study of Sulfur Dioxide, Sulfite, and Sulfonate Solutions and of the Substituted Sulfonate Ions $X_3CSO_3^-$ (X = H, Cl, F). *Inorg. Chem.* **2007**, *46*, 8332–8348.

(44) Prendergast, D.; Galli, G. X-Ray Absorption Spectra of Water from First Principles Calculations. *Phys. Rev. Lett.* **2006**, *96*, 215502.

(45) Hohenberg, P.; Kohn, W. Inhomogeneous Electron Gas. *Phys. Rev.* **1964**, *136*, B864.

(46) Kohn, W.; Sham, L. J. Self-Consistent Equations Including Exchange and Correlation Effects. *Phys. Rev.* **1965**, *140*, A1133.

(47) Paddison, S. J.; Elliott, J. A. Molecular Modeling of the Short-Side-Chain Perfluorosulfonic Acid Membrane. *J. Phys. Chem. A* **2005**, *109*, 7583–7593.

Graphical TOC Entry